Appl. Phys. A 80, 1611–1616 (2005)
DOI: 10.1007/s00339-005-3232-2

Applied Physics A
Materials Science & Processing

Rapid communication

K. WANG
C. STEIMER
D. WAMWANGI
S. ZIEGLER
M. WUTTIG✉

Effect of indium doping on $Ge_2Sb_2Te_5$ thin films for phase-change optical storage

I. Physikalisches Institut der RWTH Aachen, 52056 Aachen, Germany

Received: 18 November 2004/Accepted: 5 February 2005
Published online: 16 March 2005 • **© Springer-Verlag 2005**

ABSTRACT The influence of In doping on the crystallization kinetics of $Ge_2Sb_2Te_5$ has been investigated using four-point-probe electrical resistance measurements, grazing incidence X-ray diffraction (XRD), X-ray reflectometry (XRR), variable incident angle spectroscopic ellipsometry, a static tester, and atomic force microscopy. For a stoichiometric $Ge_2Sb_2Te_5$ alloy doped with 3% In, the amorphous-to-crystalline transition is observed at 150 °C in the sheet resistance measurements. XRD reveals the formation of a predominant NaCl-type $Ge_2Sb_2Te_5$ phase during the amorphous-to-crystalline transition together with small amounts of crystalline In_2Te_3. Density values of $5.88 \pm 0.05\ \mathrm{g\,cm^{-3}}$ and $6.22 \pm 0.05\ \mathrm{g\,cm^{-3}}$ are measured by XRR for the film in the amorphous and crystalline states, respectively. Perfect erasure can be achieved by laser pulses longer than 165 ns. The retarded crystallization, as compared with the undoped $Ge_2Sb_2Te_5$ alloy, is attributed to the observed phase segregation. Sufficient optical contrast is exhibited and can be correlated with the large density change upon crystallization.

PACS 68.55.-a; 78.20.-e; 78.66.Jg

1 Introduction

In the last decade, phase-change optical recording based upon chalcogenide glasses has advanced remarkably and full-scale commercial applications in the form of rewritable compact disks (CD-RWs), digital versatile disks (DVD-RWs), and blue-ray disks have occurred [1, 2]. The principle of phase-change optical recording is based on a thermally induced reversible transformation between an amorphous and a crystalline phase [3, 4]. Up to now, the search for recording materials possessing fast crystallization rate and long data retention has been pursued. Research results have revealed that Ge–Sb–Te compounds along the pseudo-binary GeTe–Sb_2Te_3 tie-line exhibit fast crystallization, which has been explained in terms of their single-phase NaCl-type structure by Matsunaga and Yamada [5]. However, the issues of long-term stability and optical contrast especially at shorter wavelengths remain to be solved [6, 7]. To meet both requirements, efforts have been made by using the chemical modification approach, which was proposed by Young et al. [8]. In related studies, transition metals such as Co, Ti, and Ag were introduced into $Ge_1Sb_2Te_4$ or $Ge_2Sb_2Te_5$ to improve the carrier-to-noise ratio and lifetime of the recorded bits [9, 10]. Cr was proposed to suppress the material flow in $Ge_2Sb_2Te_5$ during heating [11]. The addition of Ge or Sb to GeSbTe films was also investigated and it was found that Sb addition could effectively improve both data retention and cyclability [12–15]. Recently, it was reported that doping with oxygen and/or nitrogen improves the recording sensitivity, erasibility, and overwriting of GeSbTe alloys [16–19].

Stoichiometric compounds modified by dopants may provide a way to satisfy the compromise between crystallization rate and archival lifetime of the recording materials for optical storage applications. In this work, we focus on the investigation of the amorphous–crystalline transition in In-doped $Ge_2Sb_2Te_5$ using electrical, optical, and X-ray measurements. Finally, the influence of In doping is summarized by comparison with undoped $Ge_2Sb_2Te_5$.

2 Experiments

Thin films of $Ge_2Sb_2Te_5$ doped with In were prepared by thermal evaporation of single-element sources at a base pressure of 1×10^{-8} mbar. The evaporation rates were controlled by a quartz-crystal microbalance (FerroTec Co.) during evaporation. A temperature controller (Omron) was employed to ensure constant evaporation rates during deposition. The evaporation rates of 0.3 Å/s, 1.0 Å/s, 1.3 Å/s, and 3.7 Å/s, respectively, were measured for the individual high-purity In, Ge, Sb, and Te sources. Employing the evaporation rates, the calculated composition of $In_{0.3}Ge_2Sb_2Te_5$ films with a thickness of 70–120 nm was fabricated on glass or Si substrates. The transition temperature was determined by temperature-dependent sheet resistance measurements. The structure of the alloy was identified by grazing incidence X-ray diffraction (XRD); density and thickness changes upon crystallization were obtained from X-ray reflectometry (XRR, Philips X'Pert MPD system). The optical properties of the

✉ Fax: +49-241-8022331, E-mail: wuttig@physik.rwth-aachen.de

film in the amorphous and crystalline states were measured by a VASE ellipsometer (J.A. Woollam Co.) from 0.73 to 4 eV. Fitting of the optical spectra enabled the calculation of the optical contrast between the two states in the wavelength range from 400 to 1000 nm. Subsequently, crystallization and re-crystallization of the alloys were measured using a static tester with an objective lens of high numerical aperture (N.A. = 0.9). Finally, an atomic force microscope (AFM, Dimension 3100 from Digital Instruments) was used to identify the topography of the irradiated region.

3 Results and discussion

Figure 1 shows the sheet resistance measurement of a 100-nm $In_{0.3}Ge_2Sb_2Te_5$ film on a glass substrate at a typical heating rate of 2.5 °C/min. Heating was performed under a protective Ar atmosphere. The abrupt drop of more than three orders of magnitude in sheet resistance measurements appears at a temperature of 150 °C, which was confirmed as the amorphous-to-crystalline transition by XRD.

Figure 2 shows the XRD scans of a 100-nm $In_{0.3}Ge_2Sb_2Te_5$ film on a glass substrate in the as-deposited state and after annealing at 180 °C. All XRD measurements were performed at room temperature under a grazing angle of incidence of 0.5° to improve the signal-to-noise ratio. Figure 2a confirms that the as-deposited films are in the amorphous state. Figure 2b shows that after annealing at 180 °C crystalline $Ge_2Sb_2Te_5$ with a NaCl-type structure is generated. The lattice parameter of the NaCl-type structure is determined to be 6.000 ± 0.003 Å, which agrees well with the values between 5.988 ± 0.008 Å and 6.027 ± 0.005 Å previously reported for undoped $Ge_2Sb_2Te_5$ [20]. It confirms that the abrupt drop at 150 °C in the sheet resistance measurement corresponds to the amorphous-to-crystalline transition. Additionally, the peak in the XRD scan situated at 25.12° can be identified as the (511) reflection of β-In_2Te_3 [21]. The result indicates that probably the crystalline In_2Te_3 phase will appear during heat treatment, which was previously found to form easily upon annealing in the In–Sb–Te alloy system [22–24].

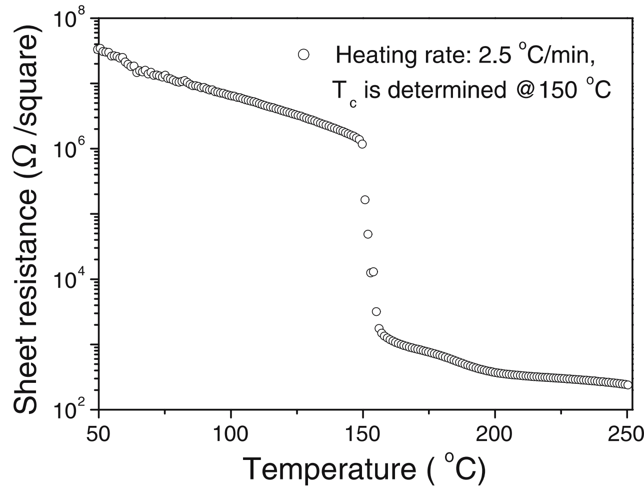

FIGURE 1 Temperature-dependent sheet resistance measurement on a 100-nm $In_{0.3}Ge_2Sb_2Te_5$ film. For a heating rate of 2.5 °C/min, the transition temperature from the amorphous to the crystalline state is determined to be 150 °C

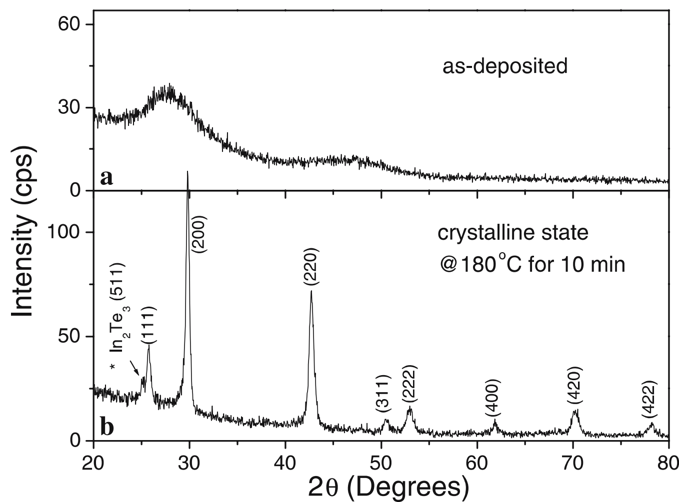

FIGURE 2 XRD scans of $In_{0.3}Ge_2Sb_2Te_5$ films in the as-deposited state (a) and annealed at 180 °C for 10 min (b). All XRD measurements are performed at room temperature under a grazing incidence angle of 0.5°

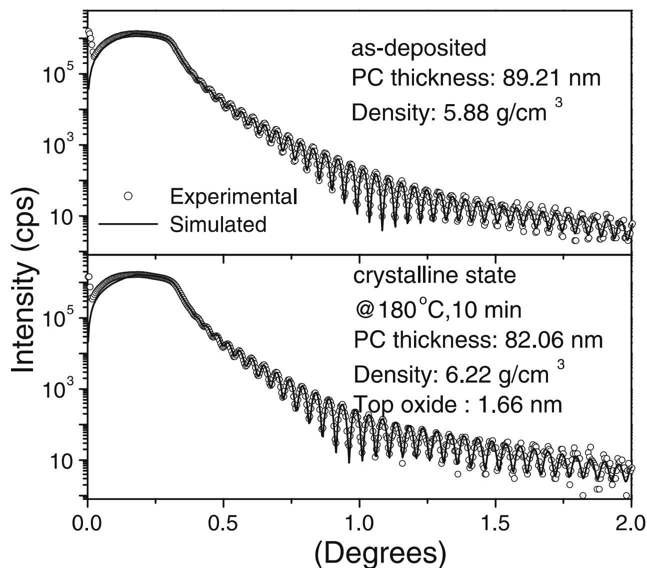

FIGURE 3 XRR measurements and the corresponding theoretical simulations for the density and thickness of $In_{0.3}Ge_2Sb_2Te_5$ films in the as-deposited and crystalline states

Figure 3 compares the XRR patterns of the films in the as-deposited state with the crystalline state. All XRR measurements are performed at room temperature. The films in the crystalline state are obtained by annealing at 180 °C for 10 min. For the annealed sample, the modulation of the oscillation amplitude indicates a second layer resulting from oxidation of the Te alloy. The XRR measurements yield a density increase of 5.78% between the amorphous and crystalline states. This corresponds to a density change from $5.88 \pm 0.05\ \mathrm{g\,cm^{-3}}$ to $6.22 \pm 0.05\ \mathrm{g\,cm^{-3}}$ upon crystallization. At the same time, the reduction in thickness is 7.08%. To obtain this value we have assumed that the oxide film on top will also contain phase-change material and have added one-half of the corresponding thickness to the total thickness of the Te alloy. To ease a comparison of the different values, the product of density and film thickness is normalized to 1.00 for the as-deposited film. The value of 0.98 for the annealed film shows that the thickness reduction compares well with the density increase. Hence, no material is lost during annealing. The density change for In-doped $Ge_2Sb_2Te_5$ is slightly smaller than the corresponding value (6.8%) in pure $Ge_2Sb_2Te_5$ [25].

Figure 4 shows the results of the ellipsometric measurements in the range from 0.73 to 4 eV together with the simulated spectra for the film in the as-deposited and crystalline states. The data were measured under three incident angles of 65°, 70°, and 75°. The Tauc–Lorentz [26] and Cauchy models [27] were employed to model the dielectric function of the phase change film and the oxidized overlayer arising from annealing, respectively. To reduce the number of the fit parameters used for the ellipsometry measurement, the thickness of the PC film and oxide layer previously acquired from XRR measurements was used as input. Satisfactory fittings were obtained by this approach.

Figure 5 depicts the optical contrast calculated from the fitted dielectric functions between the as-deposited and annealed samples from 400 to 1000 nm. Here, the optical contrast is defined as $(R_c - R_a)/R_c$, where R_a and R_c are the reflectivities of the film in the amorphous and crystalline states, respectively. From Fig. 5, we can see that the optical contrast decreases monotonically with decreasing wavelength, but the alloy exhibits a high optical contrast of more than 24% even at 400 nm. This makes the material suitable for applications at shorter wavelengths. The high optical contrast is presumably related to the pronounced density change between the amorphous and the crystalline states [28, 29].

Figure 6 displays the power–time-effect (PTE) diagram, representing the

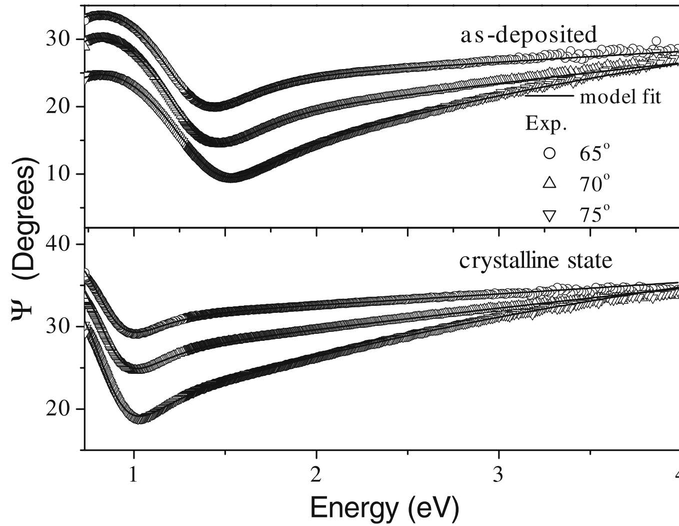

FIGURE 4 Ellipsometric analysis for the $In_{0.3}Ge_2Sb_2Te_5$ film in two states. The Tauc–Lorentz and Cauchy models were used for the PC layer and the oxidized overlayer, respectively

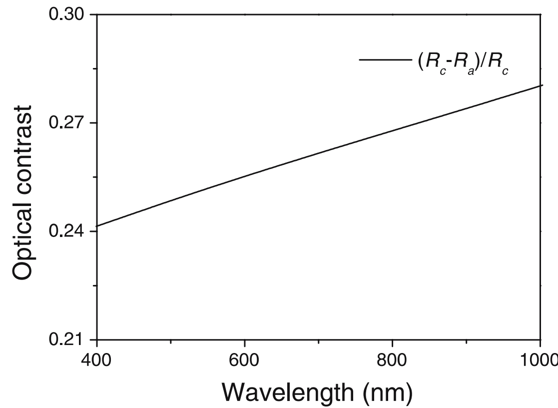

FIGURE 5 The calculated optical contrast for an 89-nm film in the wavelength range from 400 to 1000 nm

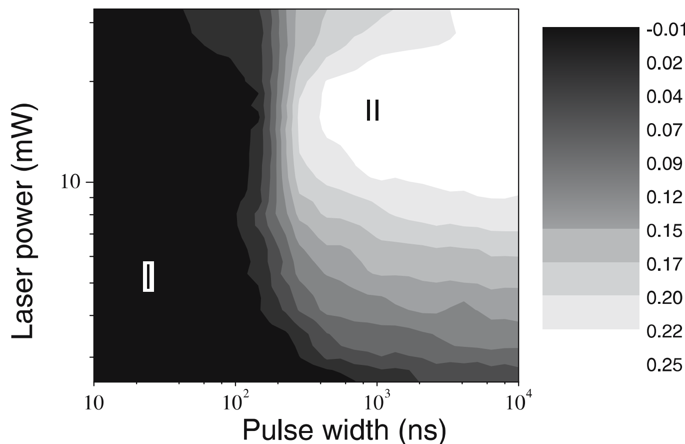

FIGURE 6 PTE diagram for the crystallization of the as-deposited 75-nm film on a Si substrate

relative reflectivity change of the film versus laser power P (2.5–32.92 mW) and pulse width t (10 ns–10 μs). The different regions characterize different levels of reflectivity change. Here the reflectivity change is defined as $\Delta R = (R_f - R_i)/R_i$, where R_i and R_f are the initial and the final reflectivities of the irradiated region, respectively. In Fig. 6, two regions of interest are distinguished: in region I, ΔR is small since the laser power was too low and/or the pulse was too short to enable crystallization. Employing higher powers and/or longer pulses, a suitable positive ΔR in region II is achieved and assigned to crystallization. The PTE diagram shows a sharp boundary between regions I and II. The position of this boundary with respect to the time axis is regarded as the incubation time. From the diagram, we can see that the minimum incubation time for crystallization in the as-deposited sample is around 250 ns, which is slow compared to the value of around 100 ns observed in undoped $Ge_2Sb_2Te_5$ [30].

Figure 7 shows an AFM image and the typical cross section of a crystalline area in region II. The bit is irradiated by an incident laser pulse of 15 mW and 1 μs. Crystallization does not only lead to a reflectivity increase but also an increase in film density. Therefore, the crystallized region corresponds to a depression in the amorphous surroundings. The modified area in Fig. 7 has a circular shape with a diameter of about 1.1 μm. The depth of the bit is 5.1 ± 0.3 nm and the thickness of the as-deposited amorphous film is 75 ± 3 nm. This leads to a change in thickness of $6.8 \pm 0.7\%$, which is in good agreement with the density change of 5.8% determined by our XRR measurements.

Figure 8 displays the PTE diagram for recrystallization, showing the relative reflectivity change of the crystalline sample upon illumination by a second laser pulse with different power P (4.5–20 mW) and pulse duration t (10 ns–10 μs). There are three regions of interest in Fig. 8. The second laser pulse is insufficient in region I to erase the amorphous bit. The reflectivity after the erase pulse is still smaller than the original one. Complete erasure is achieved in region II, where the reflectivity has increased to the original level. In region III the film is ablated, as indicated by the large decrease in reflectivity. From the PTE diagram, we can see that complete erasure of melt-quenched amorphous bits will be achieved under the laser irradiation up to 165 ns, which is obviously slower than the complete erasure time (CET) of 10 ns for $Ge_2Sb_2Te_5$ [30]. This phenomenon might be related to the segregation of crystalline In_2Te_3 in the NaCl-type $Ge_2Sb_2Te_5$ crystalline phase, identified by XRD. Hence, long-distance atomic diffusion processes required for segregation may explain the elongated time for crystallization [5, 31].

Figure 9 displays the AFM micrograph of an amorphous bit produced by the first write pulse in the crystalline matrix. The amorphous bit is created upon laser illumination with a power of 28 mW and a duration of 70 ns. Besides a decrease in reflectance, amorphiza-

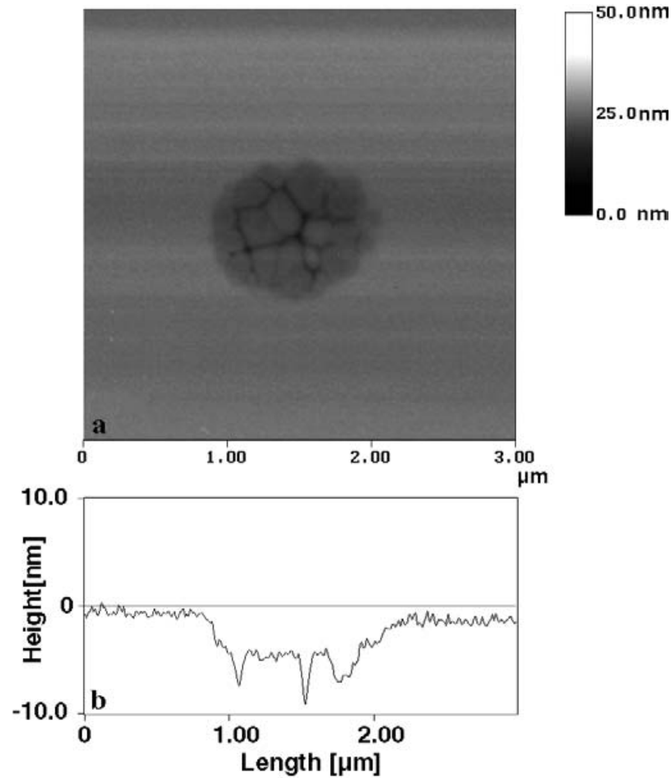

FIGURE 7 (**a**) AFM image of a crystalline bit produced by laser irradiation (power 15 mW, duration 1 μs) and (**b**) typical cross section of the crystalline bit

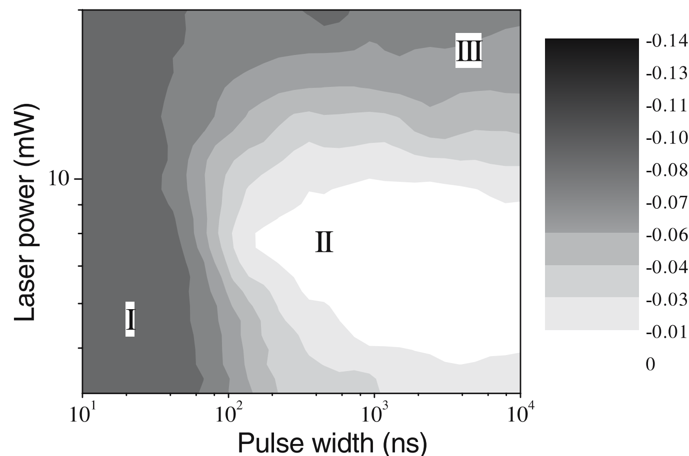

FIGURE 8 PTE diagram for the crystallization of melt-quenched amorphous bits for the annealed sample on a Si substrate. In this test, one fixed pre-pulse of 28 mW and 70 ns was first used to write an amorphous bit. A second pulse of varying power and length followed to erase the written bit. Complete erasure (zone II) can be realized up to 165 ns

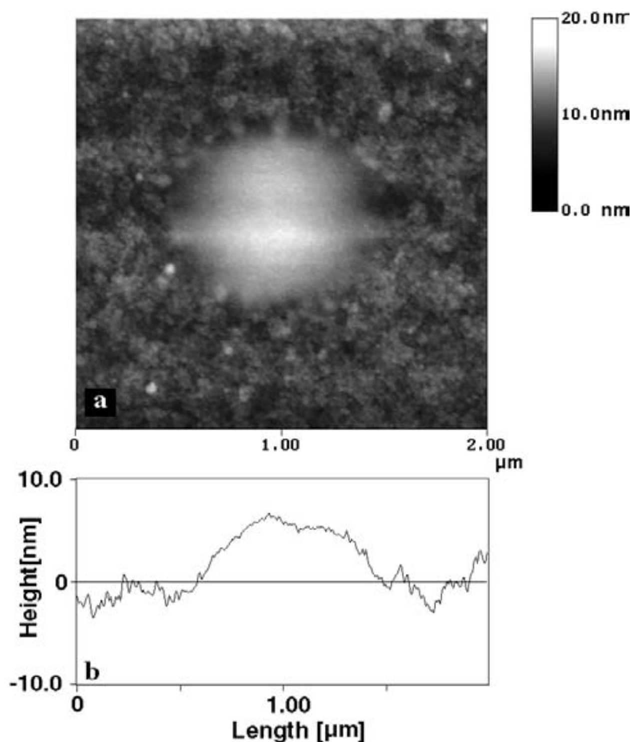

FIGURE 9 (**a**) Amorphous bit written with a laser pulse of 28 mW and 70 ns into crystalline surroundings on a Si substrate and (**b**) typical cross section of the written bit

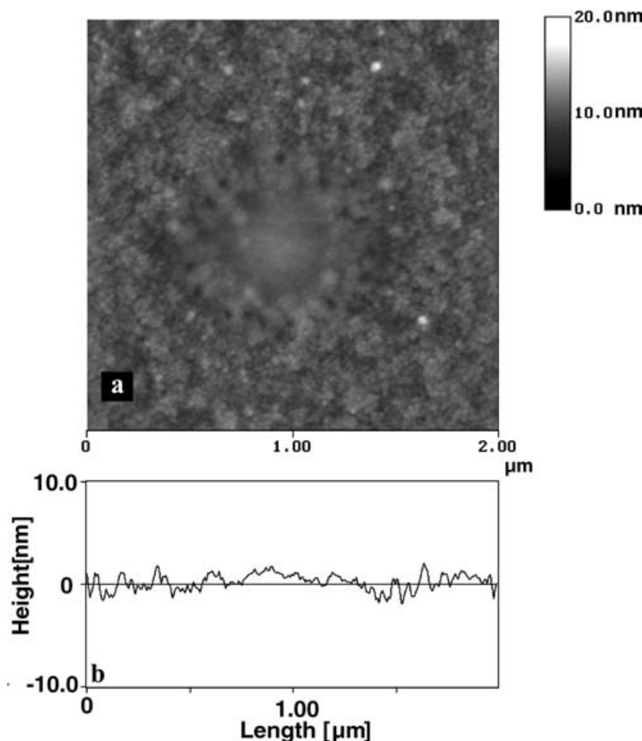

FIGURE 10 (**a**) Complete erasure by a second pulse (power 7.5 mW, duration 200 ns) and (**b**) typical cross section of the erased bit

tion also leads to a decrease in density and therefore to a local increase in film thickness. The diameter of the amorphous bit is around 900 nm and the height is approximately 5.1 nm.

Figure 10a shows the AFM micrograph of an erased bit produced by the second laser pulse. Figure 10b shows a typical cross section of a bit after the second erase pulse of 7.5 mW and 200 ns. From the image, we can see that the height of the erased bit has already recovered to the same height as the crystalline background. This indicates that complete erasure is realized, in line with the vanishing reflectance change. A decrease in roughness of the surface is observed in both the amorphized and the completely erased bits, which is related to the melt quench of the local region during the amorphization under the irradiation of a higher power laser [32].

4 Summary

In-doped $Ge_2Sb_2Te_5$ shows the same transition temperature of 150 °C for the amorphous-to-crystalline transition as the undoped alloy. XRD scans suggest that a mixed phase composed of a predominant $Ge_2Sb_2Te_5$ NaCl-type crystalline phase and a small amount of crystalline In_2Te_3 is formed during crystallization. The NaCl-type phase possesses the same lattice parameter as undoped $Ge_2Sb_2Te_5$. The optical contrast between the amorphous and crystallized states can be larger than 24% in the wavelength range from 400 to 1000 nm. This is related to the sufficient density change between the two states. A longer incubation time is observed and the crystallization speed is slowed down, which is correlated with the observed phase separation. The results indicate that In might play an important role in modifying the crystallization kinetics of Te-based phase-change materials.

ACKNOWLEDGEMENTS K. Wang would like to thank the Alexander von Humboldt-Stiftung (AvH, Germany) for a fellowship.

REFERENCES

1 T. Ohta, K. Nishiuchi, K. Narumi, Y. Kitaoka, H. Ishibashi, N. Yamada, T. Kozaki, Jpn. J. Appl. Phys. **39**, 770 (2000)
2 G.F. Zhou, Mater. Sci. Eng. A **304–306**, 73 (2001)
3 S.R. Ovshinsky, Phys. Rev. Lett. **21**, 20 (1968)
4 M. Libera, M. Chen, Mater. Res. Soc. Bull. **15**, 40 (1990)
5 T. Matsunaga, N. Yamada, Jpn. J. Appl. Phys. **41**, 1674 (2002)
6 N. Yamada, Mater. Res. Soc. Bull. **21**, 48 (1996)
7 M.H.R. Lankhorst, L. van Pieterson, M. van Schijndel, B.A.J. Jacobs, J.C.N. Rijpers, Jpn. J. Appl. Phys. **42**, 863 (2003)
8 R.T. Young, D. Strand, J. Gonzalez-Hernandez, S.R. Ovshinsky, J. Appl. Phys. **60**, 4319 (1986)

9 M. Terao, Y. Miyauchi, K. Andoo, R. Tamura: Optoelectron. Devices Technol. **4**, 223 (1989)
10 C. Lie, P. Kuo, W. Hsu, T. Wu, P. Chen, S. Chen, Jpn. J. Appl. Phys. **42**, 1026 (2003)
11 A. Hirotsune, Y. Miyauchi, M. Terao, Appl. Phys. Lett. **66**, 2312 (1995)
12 T. Matsushita, A. Suzuki, T. Kamitani, M. Okuda, Proc. SPIE **2053**, 70 (1993)
13 P.K. Khulbe, E.M. Wright, M. Mansuripur, J. Appl. Phys. **88**, 3926 (2000)
14 N. Yamada, T. Matsunaga, J. Appl. Phys. **88**, 7020 (2000)
15 S. Privitera, E. Rimini, C. Bongiorno, R. Zonca, A. Pirovano, R. Bez, J. Appl. Phys. **94**, 4409 (2003)
16 R. Kojima, T. Kouzaki, T. Matsunaga, N. Yamada, Proc. SPIE **3401**, 14 (1998)
17 G. Zhou, B.A.J. Jacobs, Jpn. J. Appl. Phys. **138**, 1625 (1999)
18 D.Z. Dimitrov, Y. Lu, M. Tseng, W. Hsu, H. Shieh, Jpn. J. Appl. Phys. **141**, 1656 (2002)
19 E. Prokhorov, G. Trapaga, E. Morales-Sanchez, M. Hernandez-Landaverde, Y. Kovalenko, J. Gonzalez-Hernandez, J. Appl. Phys. **96**, 1040 (2004)
20 I. Friedrich, V. Weidenhof, W. Njoroge, P. Franz, M. Wuttig, J. Appl. Phys. **87**, 4130 (2000)
21 *JCPDS Database* (International Center for Diffraction Data, PA, 1999), PDF 33-1488
22 Y. Maeda, H. Andoh, I. Ikuta, H. Minemura, J. Appl. Phys. **64**, 1715 (1988)
23 Y. Maeda, H. Andoh, I. Ikuta, M. Nagai, Y. Katoh, H. Minemura, N. Tsuboi, Y. Satoh, N. Gotoh, M. Ishigaki, Appl. Phys. Lett. **54**, 893, (1989)
24 L. Men, F. Jiang, F. Gan, Mater. Sci. Eng. B **47**, 18 (1997)
25 W. Njoroge, H.-W. Woltgens, M. Wuttig, J. Vac. Sci. Technol. A **20**(1), 230 (2002)
26 G.E. Jellison, F.A. Modine, Appl. Phys. Lett. **69**, 371 (1996)
27 J.A. Woollam, *Guide to Using WASE32TM* (WexTech, New York, 1995), p. 294
28 R. Detemple, D. Wamwangi, G. Bihlmayer, M. Wuttig, Appl. Phys. Lett. **83**, 2572 (2003)
29 M. Luo, M. Wuttig, Adv. Mater. **16**, 439 (2004)
30 V. Weidenhof, I. Friedrich, S. Ziegler, M. Wuttig: J. Appl. Phys. **89**, 3168 (2001)
31 J.H. Coombs, A.P.J.M. Jongenelis, W. van Es-Spiekman, B.A.J. Jacobs, J. Appl. Phys. **78**, 4918 (1995)
32 K. Wang, D. Wamwangi, S. Ziegler, C. Steimer, M.J. Kang, S.Y. Choi, M. Wuttig, Phys. Status Solidi A **201**, 3087 (2004)